Role of Asxl2 in non-alcoholic steatohepatitis-related hepatocellular carcinoma developed from diabetes

ZHIQIU HU[1,2*], ZIPING ZHANG[1,2*], FEI TENG[1,2], JINFENG FENG[1,2], XUBO WU[1,2] and QIMENG CHANG[1,2]

[1]Department of Hepatopancreatobiliary Surgery, Minhang Hospital, Fudan University;
[2]Institute of Fudan-Minhang Academic Health System, Minhang Hospital, Fudan University, Shanghai 201199, P.R. China

Received April 13, 2020; Accepted August 27, 2020

DOI: 10.3892/ijmm.2020.4782

Abstract. The present study investigated the mechanism(s) of non-alcoholic steatohepatitis-related hepatocellular carcinoma (NASH-HCC) developed from diabetes. Streptozotocin and a high-fat diet (STZ-HFD) were used to induce NASH-HCC in ApoE$^{-/-}$ mice. Mouse liver functions were evaluated by H&E staining, liver/body weight and serum biochemical analysis. The expression levels of inflammation-associated factors were determined by RT-qPCR. Gene expression profiles related to molecular functions and pathways of NASH-HCC were examined by principal component analysis, heatmap, gene ontology and KEGG pathway enrichment analysis. Differentially expressed genes (DEGs) in tumor tissues were confirmed by RT-qPCR. The expression of Asxl2 in human NASH-HCC, other HCC tissues and HCC cells was measured by western blot (WB analysis) and RT-qPCR. For SNU-182 cells transfected with siAsxl2 or Hep3B cells with Asxl2 overexpression, cell proliferation, cell cycle, migration and invasion were respectively determined by CCK-8 assays, flow cytometry, wounding healing and Transwell assays. The expression levels of cell metastasis- and cycle-related proteins were determined by WB analysis and RT-qPCR. NASH-HCC model mice exhibited tumor protrusion with severe steatosis. The blood glucose concentration, serum levels of alanine aminotransferase (ALT), aspartate aminotransferase (AST) and low-density lipoprotein (LDL), total bile acid (TBA) and the levels of interleukin (IL)-6, tumor necrosis factor (TNF)-α, glypican 3 (GPC3) and transforming growth factor (TGF)-β were all increased in NASH-HCC model mice. DEGs were mainly related to chromosome organization, the cell cycle and the mitogen-activated kinase (MAPK) pathway. Asxl2 was significantly downregulated in HCC tissues and cells, and this regulated cell growth, migration and invasion. The gene expression pattern, related molecular functions and signaling pathways of NASH-HCC differed from those of normal liver tissues. Additionally, the downregulation of Asxl2 may play a potential role in development of NASH-HCC in patients with diabetes.

Introduction

Hepatocellular carcinoma (HCC) is one of main causes of cancer-related mortality (1). Currently, the incidence of hepatitis B and C viruses (HBV and HCV)-related HCC has been greatly reduced by widely adopted HBV vaccination and curative HCV treatments; however, non-alcoholic steatohepatitis (NASH)-related HCC (NASH-HCC) is another type of HCC caused by non-alcoholic fatty liver disease (NAFLD) or NASH. NAFLD and its histological progressive form, NASH, are risk factors for the development of HCC. NAFLD, the most frequent chronic liver disease, is characterized by the accumulation of fat in the liver (2), and 4-22% of HCC cases are ascribed to NAFLD. A previous study demonstrated that increased bile acid levels promote liver carcinogenesis in a mouse model of NASH-HCC (3). Different strategies, such as, checkpoint blockade, vaccination, adoptive cell transfer, pan-tyrosine kinase inhibitors and tumor ablation have been developed for the treatment of NASH-HCC (4). However, the prevention and treatment of NASH-HCC remains a challenge due to a lack of understanding of the mechanisms underlying the development and progression of NASH-HCC.

NASH-HCC is often accompanied by a number of metabolic comorbidities, including type II diabetes (5). Diabetes/obesity accounts for 36.6% of all HCC cases, and is therefore one of the main risk factors for the development of HCC in the United States (6). In type II diabetes, the insensitivity of cells to insulin decreases glucose consumption and increases glucose levels in the blood. Notably, patients with diabetes or insulin resistance

Correspondence to: Dr Qimeng Chang, Department of Hepatopancreatobiliary Surgery, Minhang Hospital, Fudan University, 170 Xinsong Road, Minhang, Shanghai 201199, P.R. China
E-mail: chqimeng_chqm@163.com

*Contributed equally

Abbreviations: NASH-HCC, non-alcoholic steatohepatitis-related hepatocellular carcinoma; STZ-HFD, streptozotocin and a high-fat diet; DEGs, differentially expressed genes; WB analysis, western blot analysis; HCC, hepatocellular carcinoma; NAFLD, non-alcoholic fatty liver disease; NASH, non-alcoholic steatohepatitis; PVDF, polyvinylidene difluoride; SEM, standard error of mean; ANOVA, analysis of variance

Key words: diabetes, NASH-HCC, mice administered STZ-HFD, Asxl2

are more likely to develop HCC (7,8). HCV can enhance the expression levels of pathways associated with cancer and type II diabetes (9), which suggests that there is an association between type II diabetes and HCC. Research has also found that 6-27% of HCC cases are attributed to diabetes with ethnic differences (10). In addition, the long-term survival of patients with HBV-related HCC with diabetes following liver transplantation is lower than that of non-diabetic patients (11). In addition, diabetes is positively associated with mortality resulting from HCC (12,13). A previous study demonstrated that metformin inhibits high-fat diet-induced cancer progression by reducing inflammation and potentially restoring NAFLD/NASH-associated tumor surveillance in zebrafish with HCC (14). Moreover, in human NASH-HCC, the expression of the obesity-associated protein, JCAD, is upregulated, which promotes the progression of NASH-HCC by inhibiting LATS2 kinase activity (15). However, the molecular biological mechanisms connecting diabetes to NASH-HCC are not yet fully understood.

Over the past several years, different mouse models of diabetes, for example, using apolipoprotein E $(ApoE)^{-/-}$ mice, have been developed (16-18). ApoE is involved in the transport of lipoproteins in the blood and in homozygous knockout mice, for gene accumulation-induced high levels of cholesterol in the blood and atherosclerosis. Low doses of β-cell toxin streptozotozin (STZ) can induce diabetes, mimicking type I diabetes in humans. In the present study, NASH-HCC was induced via an injection of STZ and the administration of a high-fat diet (HFD) in $ApoE^{-/-}$ mice. Following a systematic investigation of the molecular biological mechanisms underlying NASH-HCC in $ApoE^{-/-}$ mice with diabetes, critical factors important for the development of NASH-HCC were identified. The present study aimed to provide a comprehensive understanding of NASH-HCC developed from diabetes.

Materials and methods

Mouse model of NASH-HCC. $ApoE^{-/-}$ (7 weeks of age, n=15) mice were bred at a constant temperature (23±1˚C) with 55±15% humidity and a 12-h light-dark cycle (lights on 09:00 to 21:00) in a typical SPF laboratory animal room at the Animal Center of Guangdong Medical Laboratory, and $ApoE^{-/-}$ male mice (8 weeks of age, n=3) were then mated with $ApoE^{-/-}$ female mice (8 weeks of age, n=12). After birth, only male mice were selected. There were 2 research groups, namely, the STZ-HFD group and the STZ-NC group, with 10 male mice were in each group. The mice in the STZ-HFD group were injected with 0.1 M sodium citrate-hydrochloric acid buffer with 150 μg STZ (S0130; Sigma-Aldrich; Merck KGaA) 5 days after birth, and were then fed a HFD (1055.05 Kcal/100 g; protein, 19.2%; fat, 4.3%; carbohydrates, 67.3%) beginning from the age of 4 weeks. The mice in the STZ-NC group were injected with 0.1 M sodium citrate-hydrochloric acid buffer at 5 days after birth, and fed a diet of 404 kcal/100 g (water, 10%; protein, 25.0%; fat, 4.5%; ash, 6.7%; carbohydrate, 49.3%; and fiber, 4.5%) beginning from the age of 4 weeks.

The mice from the STZ-HFD and STZ-NC groups (10 mice in each group) were sacrificed at the age of 22 weeks. Mouse serum was prepared for serum biochemical analysis, and liver tissues were isolated for weighing, histological, biochemical and molecular biological analysis. NASH-HCC [tumor (T)], non-cancerous matched tissues (STZ-HFD) and normal liver tissues (STZ-NC) were, respectively, collected for RT-qPCR and RNA-sequencing. The animal experiments were performed according to the guidelines of the Minhang Hospital Animal Ethics Committee. Efforts were made in consideration of animal welfare.

Patients and tissue samples. A total of 42 cases of NASH-HCC (age, 35-72 years; female, n=20; male, n=22), 45 cases of other types of HCC (age, 43-68 years; female, n=23; male, n=22) and non-cancerous matched tissues (n=42, NASH-HCC adjacent tissues; n=45). HCC adjacent tissues were respectively collected from patients with NASH-HCC or other types of HCC during surgery at the Minhang Hospital from May 1, 2016 to May 1, 2018. The samples were frozen in liquid nitrogen and maintained at -80˚C. The present study was approved by the Ethics Committee of Minhang Hospital and written informed consent was signed by each participant prior to surgery.

Cells and cell culture. Human liver epithelial cells (THLE-2, CBP61031) and the human liver cancer cell lines, SNU-182 (CBP60211), SNU-387 (CBP60214), Hep3B (CBP60197) and PLC/PRF/5 (CBP60223), were purchased from Nanjing Cobioer BioScience Co., Ltd. The human liver cancer cell line, SK-Hep1 (HTB-52), was obtained from the American Tissue Culture Collection (ATCC). THLE-2 cells were cultured in Dulbecco's modified Eagle's medium (DMEM, 10566024; Gibco; Thermo Fisher Scientific, Inc.) supplemented with 10% fetal bovine serum (FBS, 16140071; Gibco; Thermo Fisher Scientific, Inc.), 100 IU/ml penicillin and 100 μg/ml streptomycin (15070063; Gibco; Thermo Fisher Scientific, Inc.). The SNU-182, SNU-387 and PLC/PRF/5 cells were cultured in RPMI-1640 medium (61870044; Gibco; Thermo Fisher Scientific, Inc.) with 10% heat-inactivated FBS in 5% CO_2. The SK-Hep1 and Hep3B were grown in DMEM supplemented with 10% FBS, 2 mM L-glutamine (4 mM, 25030081; Gibco; Thermo Fisher Scientific, Inc.), penicillin and streptomycin.

Liver/weight body ratio and histopathology. The mouse livers were collected, observed, weighed and photographed. Liver organ index was determined based on the liver weight (g)/the body weight of the mice (g). One part of the liver tissues was snap-frozen in liquid nitrogen for further experiments, while another part was fixed with 10% formalin for liver histopathological analysis by H&E staining. For H&E staining, the tissue blocks (3-5 μm thick) were cut using a freezing microtome. Specifically, the samples were fixed in 10% (v/v) neutral-buffered formaldehyde (G2161, Beijing Solarbio Science & Technology Co., Ltd.), rinsed in PBS, and then orderly stained with hematoxylin and eosin (C0105; Beyotime Institute of Biotechnology, Inc.) for 10 min at room temperature, and washed with distilled water for 10 min. Finally, images of the sections was captured using a light microscope (E200; Nikon Corporation) at x40, x100 and x400 magnification.

Serum biochemical analysis. The blood samples were separately obtained via tail vein puncture from 5 mice in each group at 6, 10, 14, 16 and 22 weeks of age. Blood glucose

Table I. Primers used for RT-qPCR.

Gene	Forward	Reverse
Ubc (mouse)	GAGGTTGCTGAGACTCGTCC	CCATCTACTGTTATCACTCGGCT
Asxl2 (mouse)	TGTCCCAGTAGTTCCTCAGTC	TGGGTTTCATGGTGATAAGCTC
Asxl2 (human)	GGAAAAGGGACGTAGGAAGAAG	ACTCATGGGTGTATTGGGGTA
HOMER1	CCCTCTCTCATGCTAGTTCAGC	GCACAGCGTTTGCTTGACT
XPO1 (mouse)	GGGTAACTCGCGGCCTAAAC	AGGGCTTCGGGAAAAGTCAC
cbx5 (mouse)	GTGGTGGAAAAGGTGTTGGAC	GTTCCCAAGTATTGTGCTCCTC
NSD1 (mouse)	TCCGGTGAATTTAGATGCCTCC	CGGTAACTGCATAGTACACCCAT
MMP-2 (human)	TACAGGATCATTGGCTACACACC	GGTCACATCGCTCCAGACT
MMP-9 (human)	TGTACCGCTATGGTTACACTCG	GGCAGGGACAGTTGCTTCT
cyclin D1 (human)	GCTGCGAAGTGGAAACCATC	CCTCCTTCTGCACACATTTGAA
c-Myc (human)	GGCTCCTGGCAAAAGGTCA	CTGCGTAGTTGTGCTGATGT
IL-6 (mouse)	CTGCAAGAGACTTCCATCCAG	AGTGGTATAGACAGGTCTGTTGG
TNF-α (mouse)	CAGGCGGTGCCTATGTCTC	CGATCACCCCGAAGTTCAGTAG
GPC3 (mouse)	CAGCCCGGACTCAAATGGG	GCCGTGCTGTTAGTTGGTATTTT
p65 (mouse)	TGCGATTCCGCTATAAATGCG	ACAAGTTCATGTGGATGAGGC
MCP-1 (mouse)	TAAAAACCTGGATCGGAACCAAA	GCATTAGCTTCAGATTTACGGGT
TGF-β (mouse)	CCACCTGCAAGACCATCGAC	CTGGCGAGCCTTAGTTTGGAC
Collagen type 1 (mouse)	GCTCCTCTTAGGGGCCACT	ATTGGGGACCCTTAGGCCAT
Collagen type 3 (mouse)	CTGTAACATGGAAACTGGGGAAA	CCATAGCTGAACTGAAAACCACC
Gapdh (mouse)	AATGGATTTGGACGCATTGGT	TTTGCACTGGTACGTGTTGAT
Gapdh (human)	TGTGGGCATCAATGGATTTGG	ACACCATGTATTCCGGGTCAAT

levels were determined using glucose strips (107233294888; Roche Diagnostics) at room temperature. Serum was then collected following centrifugation at 850 x g for 15 min at room temperature. A fully-automatic biochemical analyzer (BS-420; Mindray Medical International Co. Ltd.) was used to detect the contents of the liver injury markers, alanine aminotransferase (ALT), aspartate aminotransferase (AST), triglycerides (TGs), low-density lipoprotein (LDL), total bile acid (TBA) and total cholesterol (TC) in serum according to the specifications and instructions of the manufacturer.

RNA isolation and RT-qPCR. For the extraction of RNA from the tissues, the tissue specimens were disrupted in liquid nitrogen, homogenized using TRIzol reagent (15596018, Invitrogen; Thermo Fisher Scientific, Inc.) at 4˚C, followed by centrifugation at 500 x g at 4˚C for 15 min. The supernatant was then collected and total RNA was isolated from the supernatant using the Qiagen RNeasy Plus Mini kit (74134; Qiagen GmbH) at 4˚C. For RNA extraction from the HCC cell lines, the cells were treated with TRIzol reagent and RNA was extracted using chloroform and isopropanol at 4˚C. The concentration of the RNA was determined using a NanoDrop 8000 spectrophotometer (ND-8000-GL; Thermo Fisher Scientific, Inc.). Reverse transcription was performed using the PrimeScript™ II 1st Strand cDNA Synthesis kit (6210B; Takara Bio, Inc.). SYBR®-Green PCR Master Mix (4312704; Applied Biosystems) and the Bio-Rad CFX 96 Touch Real-Time PCR Detection System (1855196; Bio-Rad Laboratories, Inc.) were employed for RT-qPCR, which was conducted at 95˚C for 5 min, 40 cycles at 95˚C for 15 sec, at 60˚C for 30 sec, and at 70˚C for 10 sec. GAPDH was used as an internal control, and the $2^{-\Delta\Delta Cq}$ method (19) was used to calculate the relative expression levels. All the reactions were performed 3 times. The primers used are listed in Table I.

Bioinformatics analysis of RNA-sequencing data. Raw sequence data were processed using the standard Illumina pipelines for base-calling and FASTQ file generation. Paired-end reads were mapped to the *Musculus* reference genome and transcriptome (build mm10) using Burrows-Wheeler Aligner (BWA). FeatureCounts (version 1.4.6-p5) was used to assign sequence reads to genes (20). Differential expression analysis was conducted using Bioconductor edgeR package 1.6 (21). Differentially expressed genes (DEGs) were determined according to an adjusted P-value <0.05 based on the Benjamini-Hochberg multiple-testing correction and the absolute value of log2-transformed fold change >2. Principle Component Analysis (PCA) was performed to evaluate the determination of associations by total gene content using FactoMineR and Factoextra R packages. The gene ontology (GO) analysis for examining molecular function was performed using EnrichR. Heatmap analysis for the top 16 DEGs was conducted by the DEGseq test after the median center had been transformed in MultiExperiment Viewer software (22). Pathway analysis employed the KEGG database (https://www.genome.jp/kegg/). KOBAS software (version v2.0) (23) was used to examine the statistical enrichment of DEGs in the KEGG pathways.

Cell transfection. siRNA targeting Asxl2 (AM16708, Sigma-Aldrich; Merck KGaA) (forward, 5'-AUACAAUUU ACUCAAUGUGAA-3'; and reverse, 5'-CACAUUGAGUAA

AUUGUAUUG-3') and negative control siRNA (A06001; GenePharma) were transfected into SNU-182 cells according to the instructions of the manufacturers. The full-length sequence of Asxl2 was amplified and cloned into the pcDNA 3.1 plasmid (V79020; Invitrogen; Thermo Fisher Scientific, Inc.). The pcDNA 3.1- Asxl2 or pcDNA 3.1 empty plasmid were then transfected into the Hep3B cells. Opti-MEM (11058021; Invitrogen; Thermo Fisher Scientific, Inc.) mixed with Lipofectamine® 2000 (11668019; Invitrogen; Thermo Fisher Scientific, Inc.) was used for the transfection of siRNAs or plasmids (50 pmol) into the cells at room temperature for 10 min. Following incubation at 37˚C for 24 h, the medium was refreshed and the cells were prepared for use in further experiments.

Western blot (WB) analysis. For WB analysis, total protein samples were extracted from the cells using RIPA lysis buffer (89901; Thermo Fisher Scientific, Inc.) with a protease inhibitor (36978; Thermo Fisher Scientific, Inc.). The Pierce™ BCA Protein Assay kit (23225; Thermo Fisher Scientific, Inc.) was used for detecting the protein concentration. Protein (60 μg/lane) was separated on 8% SDS-polyacrylamide gels and then transferred onto a polyvinylidene difluoride (PVDF) membrane (LC2002; Invitrogen; Thermo Fisher Scientific, Inc.), which was blocked with 5% skimmed milk (PA201-01; HBM BioMed China Ltd.) for 10 min at room temperature. The PVDF membrane was then incubated with primary antibodies at 4˚C overnight. Primary antibodies used were as follows: Anti-Asxl2 (ab176599, 1:2,000), anti-matrix metalloproteinase (MMP)-2 (ab37150, 1:2,000), anti-MMP-9 (ab73734, 1:2,000), anti-cyclin D1 (ab134175, 1:2,000), anti-c-Myc (ab32072, 1:2,000), anti-GAPDH (ab8245, 1:5,000) (all from Abcam). The membrane was further incubated with HRP-linked anti-rabbit IgG antibody (1:2,000, 7074; Cell Signaling Technology, Inc.) for ZEB1 and GAPDH at 4˚C overnight. Finally, SignalFire™ ECL reagent (6883; Cell Signaling Technology, Inc.) and ImageQuant ECL Imager (28-9605-63; GE Healthcare) were employed for signal detection. ImageLab software (version 5.0; Bio-Rad Laboratories, Inc.) was used to analyze according to grayscale value. Prior to each incubation, 1X TBST (50 mM Tris, 150 mM NaCl and 2% Tween-20; pH 7.5) was used to wash the membrane 3 times. GADPH served as an internal control.

Cell Counting kit (CCK)-8 assay. The transfected cells at 2,000 cells per well were seeded into 96-well plates. Following incubation for 24, 48, 72 or 96 h at 37˚C, the wells were rinsed with PBS. Subsequently, 20 μl cell CCK-8 reagent (70-CCK801; MultiSciences Biotech Co. Ltd.) mixed with 100 μl fresh culture were added to each well. Following incubation for 4 h at 37˚C in a 5% CO_2 atmosphere, cell viability was measured by reading the optical density value (DG-3022A microplate reader; Nanjing Huadong Electron Tube Factory) at a wavelength of 450 nm. All the experiments were performed in triplicate.

Flow cytometry. The cells were first trypsinized at 37˚C for 2 min, collected by centrifugation at 500 x g at 4˚C for 5 min, washed twice with 300 μl PBS and then fixed in 700 μl ethanol at -20˚C overnight. The cells were then stained with 1 μg/ml of propidium iodide (PI, 25535-16-4; Aladdin, China) in 1 ml of PBS containing 50 μg/ml RNase A for 30 min at 4˚C in the dark and subsequently subjected to flow cytometry (FACSCalibur flow cytometer; BD Biosciences) and data were analyzed using FlowJo software (version 7.6.1; FlowJo LLC). The experiment was repeated 3 times.

Wounding-healing assay. The cells ($5.0x10^5$ cells/well) were cultured in 6-well plates (140660; Thermo Fisher Scientific, Inc.) at 37˚C until cells appeared contact inhibition. The cells were then scratched with a 10-μl micropipette tip. After washing the cells twice with 1X PBS, the cells were starved by the addition of fresh medium without FBS into the plates. Subsequently, the cells were transfected with siRNA or plasmids for 48 h as described above. Images of wound healing were captured using a microscope (TS100; Nikon Corporation) at 0 and 48 h. The average horizontal migration rate was calculated according to the formula: $(width^{0\,h}\text{-}width^{24\,h})/width^{0\,h}$ x100%.

Transwell assay. The cells ($5.0x10^5$ cells/well) were seeded into Matrigel invasion chambers (3428; Corning, Inc.). Following incubation at 37˚C for 24 h, the invaded cells were fixed with methanol (M116127; Aladdin, China) and stained with 0.1% crystal violet (548-62-9; Aladdin, China) at room temperature for 15 min. The number of invasive cells was counted under a microscope (TS100; Nikon Corporation).

Statistical analysis. The data are presented as the means ± standard error of mean (SEM) and analyzed by one-way analysis of variance (ANOVA), followed by Dunnett's post hoc test or Tukey's test. $P<0.05$ was considered to indicate a statistically significant difference. GraphPad Prism 6 software (GraphPad Prism, Inc.) was used to perform the statistical analyses.

Results

Liver pathology and biochemical parameters of normal mice and mice in the NASH-HCC model group. By combining chemical and dietary interventions, a simple model system using diabetic $ApoE^{-/-}$ mice was successfully induced to establish the model of NASH-HCC. Macroscopically, the livers from NASH-HCC model mice (STZ-HFD) exhibited a pale yellow color, mild swelling and tumor protrusion at 20 weeks (Fig. 1A). H&E staining also revealed fatty liver with severe steatosis in the NASH-HCC model mice, with inflammatory foci and moderate inflammatory infiltration, including neutrophils, lymphocytes and monocytes (Fig. 1B). The concentration of blood glucose in the NASH-HCC model mice was significantly higher than that in normal mice (STZ-NC, $P<0.05$, Fig. 1C). Moreover, no significant differences in liver/weight index between the NASH-HCC model mice and the normal mice ($P>0.05$, Fig. 1D) were identified. Furthermore, the serum levels of ALT, AST, TG, LDL, TBA and TC in the NASH-HCC model mice and normal mice were determined, and it was found that the serum levels of ALT, AST, LDL and TBA in the NASH-HCC model mice were higher than those in the normal mice ($P<0.05$; Fig. 1E-J).

Expression levels of pro-inflammatory factors in normal, NASH-HCC and non-cancerous matched tissues. Subsequently,

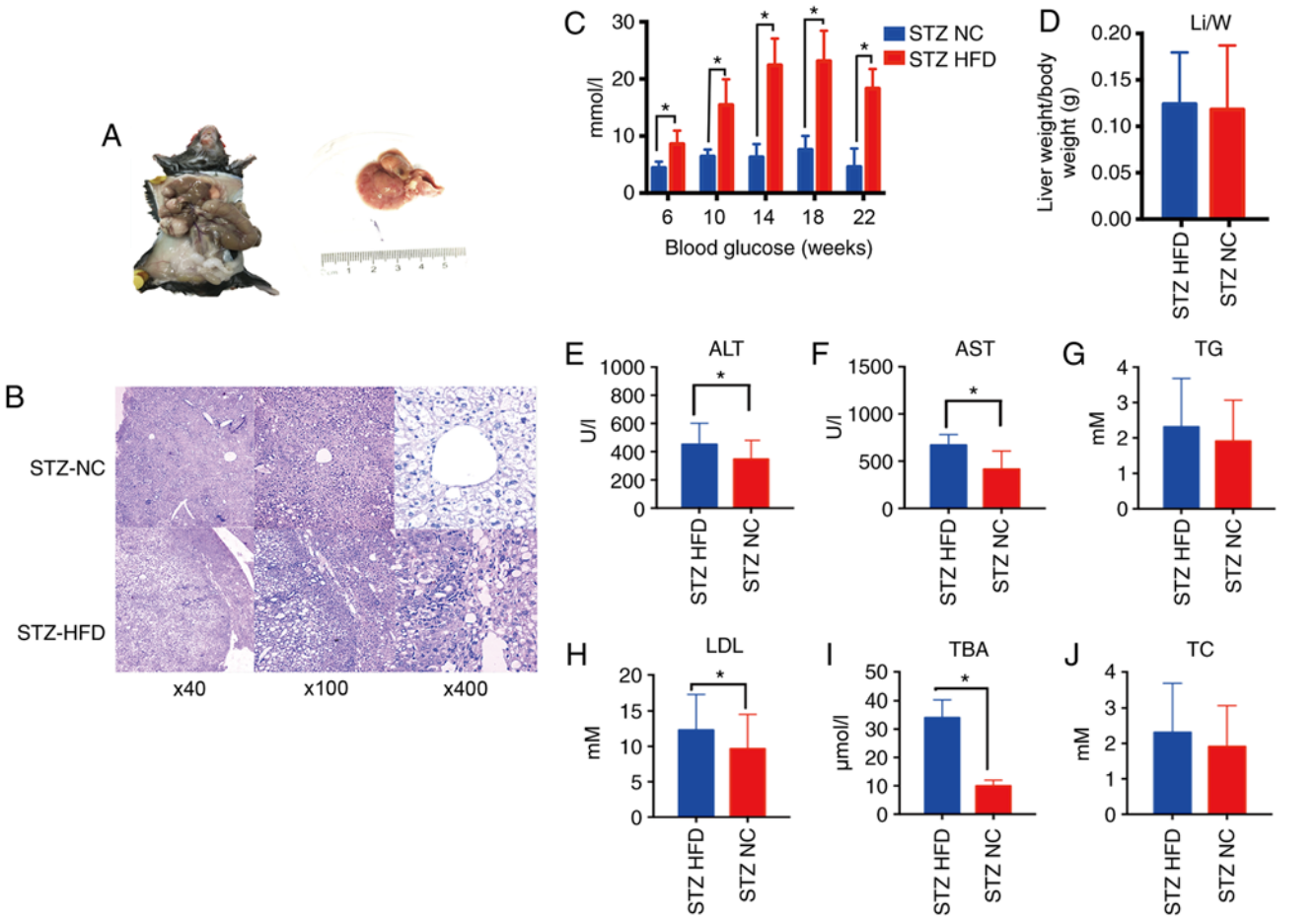

Figure 1. Pathophysiological features and biochemical analysis of normal and NASH-HCC tissues. (A) STZ-HFD group general view. (B) H&E was used to stain the liver sections from mice in the STZ-HFD group (week 22) and STZ-NC group (week 22). Original magnifications x40, x100 and x400. (C) The concentrations of blood glucose in mice after feeding the mice for 6, 10, 14, 18 and 22 weeks were measured using a blood glucose meter. (D) The liver (g) body weight (g) determined in STZ-HFD mice (week 22) and STZ-NC mice (week 22). (E-J) Serum levels of ALT, AST, TG, LDL, TBA and TC were measured using a biochemical analyzer. *P<0.05 vs. NC group. STZ, streptozotocin; HFD, high-fat diet; NC, negative control; ALT, alanine aminotransferase; AST, aspartate aminotransferase; TG, triglyceride; LDL, low-density lipoprotein; TBA, serum total bile acid; TC, total cholesterol.

the expression levels of pro-inflammatory cytokines [interleukin (IL)-6, tumor necrosis factor (TNF)-α and transforming growth factor (TGF)-β], pro-inflammatory chemokines [monocyte chemoattractant protein-1 (MCP-1)], pro-inflammatory signaling intermediates [glypican 3 (GPC3), p65], collagens (collagen type 1 and collagen type 3) in normal (STZ-NC), NASH-HCC (T) and non-cancerous matched tissues (STZ-HFD) were measured. The results of RT-qPCR revealed that the expression levels of IL-6, TNF-α and GPC3 were significantly increased in both the NASH-HCC and non-cancerous matched tissues (all P<0.05; Fig. 2A-C). p65 expression was found to be significantly downregulated, while that of MCP-1, collagen types 1 and 3 was markedly upregulated in the non-cancerous matched tissues (all P<0.05; Fig. 2D, E, G and H). The results also demonstrated that TGF-β expression was specifically upregulated in the NASH-HCC group, whereas that of collagen type 3 was noticeably downregulated (both P<0.05; Fig. 2F and H).

DEGs, molecular functions and pathways enriched in NASH-HCC. To elucidate the molecular basis for hepatocarcinogenesis in NASH-HCC, gene expression profiles in NASH-HCC, non-cancerous matched tissues (NCMTs) and normal tissues were compared by RNA-seq analysis. According to the results of PCA, the NASH-HCC samples and normal tissues were clustered, respectively, to themselves; therefore, the samples from different tissues were distinguished (Fig. 3A). GO molecular functional analysis of all DGEs in the tumor tissues was mainly related to chromosome organization, mitotic nuclear division, chromatin modification, DNA repair, mRNA processing and chromosome segregation (Fig. 3B). Furthermore, the heatmap revealed the 5 most differentially upregulated and 11 most differentially downregulated genes in NASH-HCC in comparison with the normal tissues (Fig. 3C). To further investigate the signaling networks enriched in NASH-HCC, KEGG pathway analysis was conducted on the DEGs in NASH-HCC in comparison with those in normal tissues, and it was found that the DEGs in NASH-HCC were significantly related to the cell cycle, mitogen-activated protein kinase (MAPK) signaling pathways, platinum drug resistance and the Fanconi anemia pathway (Fig. 3D).

It was considered that Ubc, Asxl2, HOMER1, XPO1, cbx5 and NSD1 had a close association with cancer. Therefore, the expression levels of Ubc, Asxl2, HOMER1, XPO1, cbx5 and NSD1 in the normal, NASH-HCC and non-cancerous matched tissues were further measured by RT-qPCR. The data

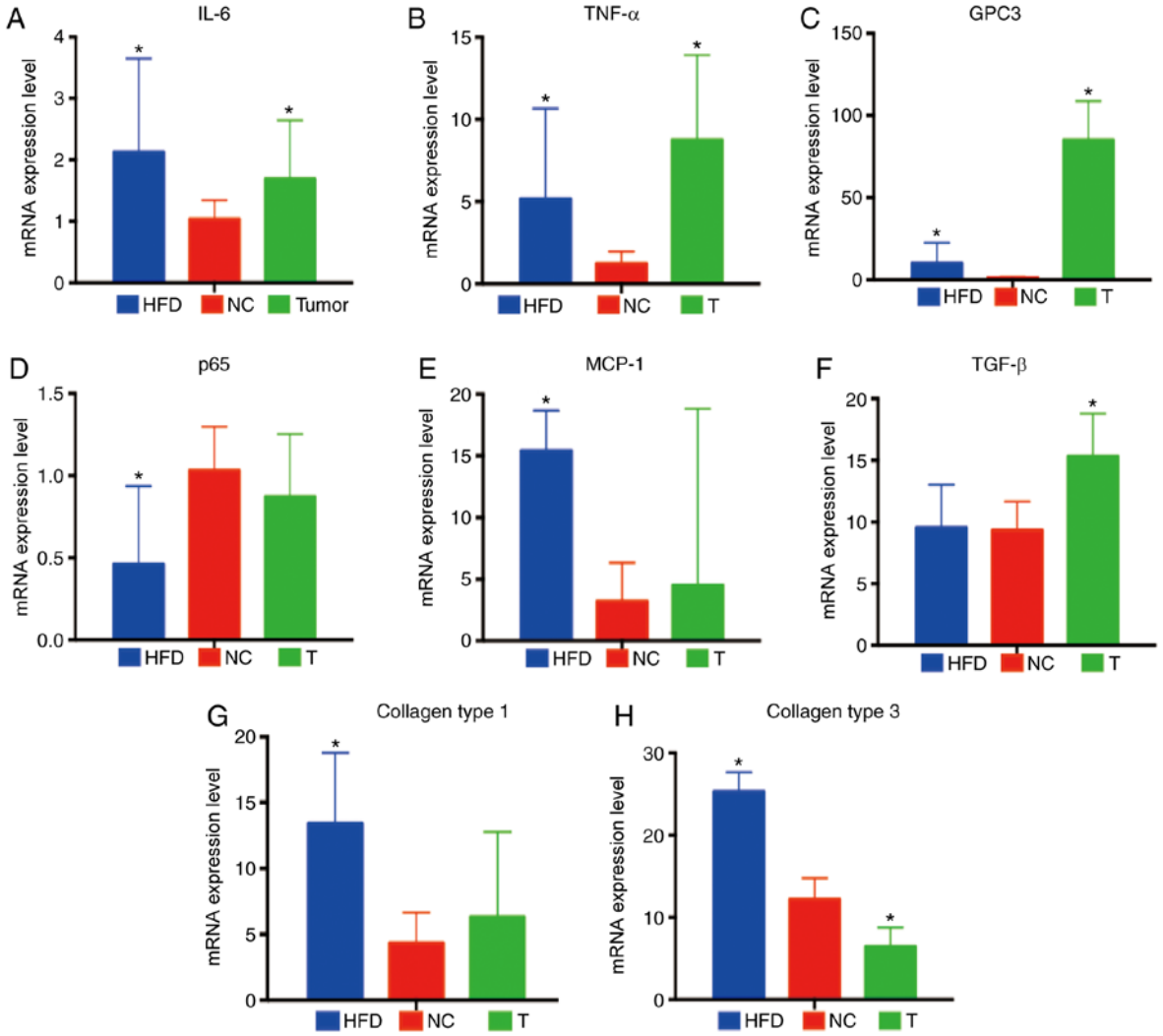

Figure 2. Inflammation-associated factors in normal, NASH-HCC and non-cancerous matched tissues. (A-H) Expression levels of IL-6, TNF-α, GPC3, p65, MCP-1, TGF-β, collagen type 1, collagen type 3 in the liver and tumor tissues of STZ-HFD mice were measured by RT-qPCR in comparison with normal liver tissues of mice in the STZ-HFD group (week 22). Data are the means ± SD (n=3/each group). *P<0.05 vs. NC group. NASH, non-alcoholic steatohepatitis; HCC, hepatocellular carcinoma; STZ, streptozotocin; HFD, high-fat diet; NC, negative control.

revealed that Ubc expression was significantly upregulated in the tumor and non-cancerous matched tissues, as compared with normal tissues, and that the expression of Ubc was the highest in tumor tissues (both P<0.001; Fig. 4A). The expression levels of Asxl2, HOMER1, XPO1, cbx5 and NSD1 were significantly downregulated in the tumor and non-cancerous matched tissues, and the expression of Asxl2, which increased approximately 8-fold, was the most downregulated gene in the tumor tissues (all P<0.001; Fig. 4A). Asxl2 is frequently mutated in patients with acute myeloid leukemia. A recent study demonstrated that the loss of Asxl2 caused myeloid malignancies in mice (24). More importantly, Asxl2 regulates glucose and lipids (25), which are both important factors for the development of diabetes and NASH-HCC. Therefore, the present study wished to further investigate the role of Asxl2 in NASH-HCC developed from diabetes.

Asxl2 expression is downregulated in human NASH-HCC and HCC tissues, and HCC cell lines. The expression levels of Asxl2 in human NASH-HCC and HCC tissues, and HCC cells were detected by RT-qPCR. It was observed that Asxl2 expression was significantly higher in the NASH-HCC adjacent tissues and HCC adjacent tissues than in the NASH-HCC and HCC tissues (both P<0.001; Fig. 4B). As measured by WB analysis and RT-qPCR, Asxl2 expression was similarly downregulated in HCC cells (Fig. 4C-E). As the expression of Asxl2 was relatively the highest in SNU-182 cells and the lowest in Hep3B cells among the 5 HCC cell lines examined, the SNU-182 and Hep3B cells were selected for use in further experiments.

Asxl2 regulates the growth, migration and invasion of SNU-182 and Hep3B cells. In order to investigate the role of Asxl2 in SNU-182 and Hep3B cells, overexpression plasmids of siAsxl2 and Asxl2 were respectively transfected into SNU-182 and Hep3B cells, and it was observed that Asxl2 expression was significantly downregulated in the SNU-182 cells by siAsxl2, but was markedly upregulated in the Hep3B cells by Asxl2 overexpression (both P<0.001; Fig. 5A and B). The proliferation of the SNU-182 cells was promoted following transfection with siAsxl2, while that of the Hep3B cells was suppressed by Asxl2 overexpression (both P<0.001 at 48 h; Fig. 5C and D).

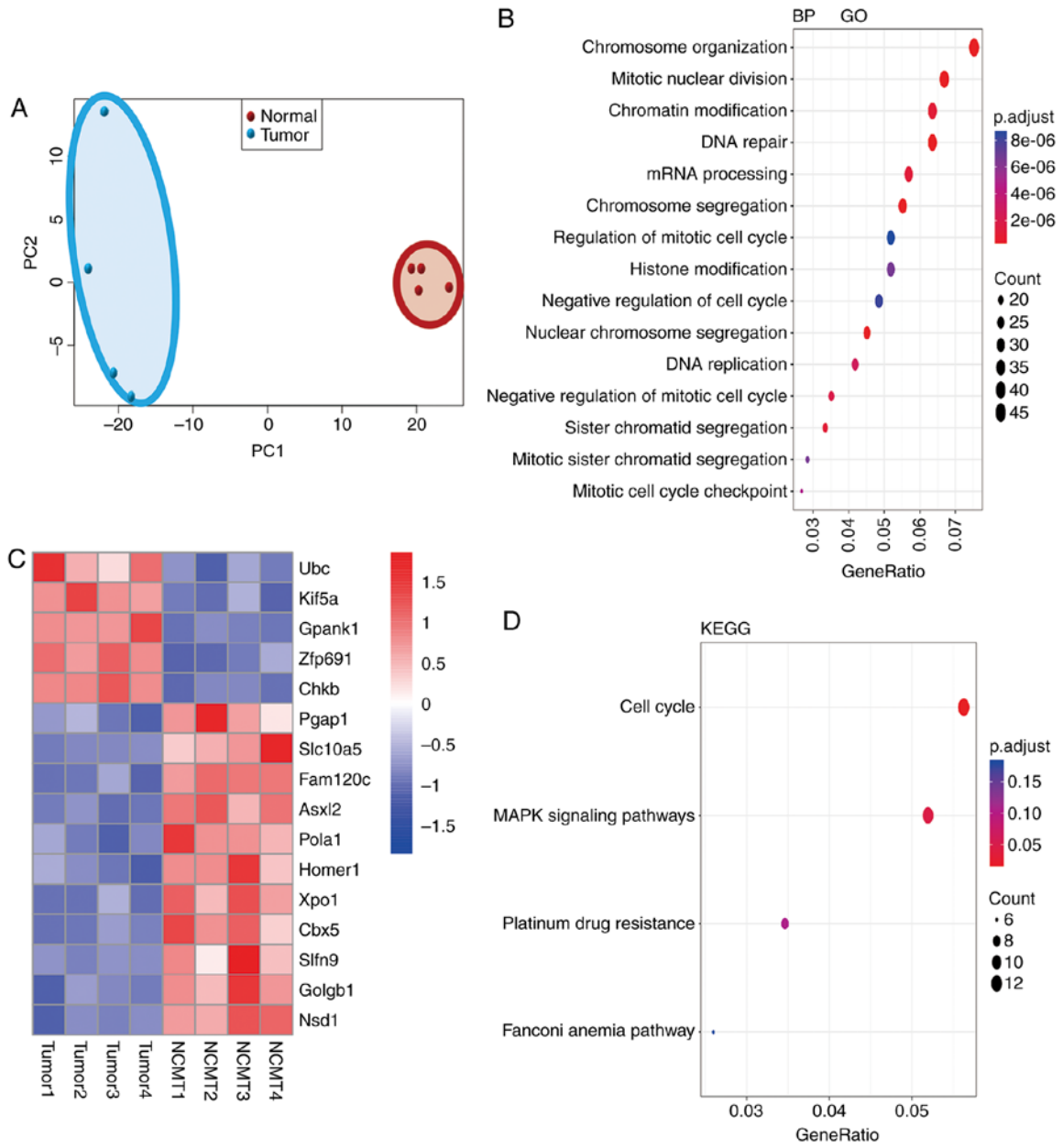

Figure 3. Aberrant gene expression, associated molecular functions and pathways in NASH-HCC compared with normal tissues. (A) PCA analysis sorted liver from normal (STZ-NC, n=4) and NASH-HCC [tumor tissue (T), n=4]. Genes were plotted in 2D visualization, indicating that samples within each group shared more similarity. The red dots in the red circle showed the PCA values of 4 normal samples and the blue dots in the blue circle indicate the PCA value of 4 tumor samples. (B) Gene ontology (GO) ana1lysis for the differentially expressed genes (DGEs) in NASH-HCC (T), as compared with normal tissues (n=4). p.adjust is the corrected P-value by the multiple hypothesis test. p.adjust $<2e^{-6}$ indicates significant differences. The black dots indicate the numbers of DEGs. (C) The DEGs in NASH-HCC (tumors, T), as compared with normal tissues (n=4). The fold change cut-off was 1.5. (D) KEGG pathway enrichment for DEGs in NASH-HCC. GeneRatio indicates the ratio of DEGs number in a certain pathway to the number of all annotated genes in this pathway. p.adjust was corrected P-value by multiple hypothesis test. p.adjust <0.05 indicated significant differences. The black dots indicate the numbers of DEGs. NASH, non-alcoholic steatohepatitis; HCC, hepatocellular carcinoma; STZ, streptozotocin; HFD, high-fat diet; NC, negative control.

CCK-8 assays also revealed that Asxl2 knockdown accelerated the cell cycle with an increase in the number of cells in the S/G2 phase, and Asxl2 overexpression induced cell cycle arrest at the G1 phase (all P<0.001; Fig. 5E and F). In addition, Asxl2 knockdown promoted the migration and invasion of the SNU-182 cells (both P<0.001; Fig. 6A and C), while Asxl2 overexpression suppressed the migration and invasion of Hep3B cells (both P<0.001; Fig. 6B and D). Moreover, the expression levels of proteins related to cell metastasis and the cell cycle in SNU-182 and Hep-3B cells were measured by WB analysis and RT-qPCR. The results revealed that the expression levels of cell cycle- related proteins were promoted by Asxl2 knockdown, whereas they were suppressed by Asxl2 overexpression (all P<0.001; Fig. 7).

Discussion

There is mounting evidence to indicate that diabetes is closely related to NASH-HCC. However, little is known about the molecular biological mechanisms of NASH-HCC developed from diabetes. In the present study, a mouse model of NASH-HCC was established and a series of DEGs were

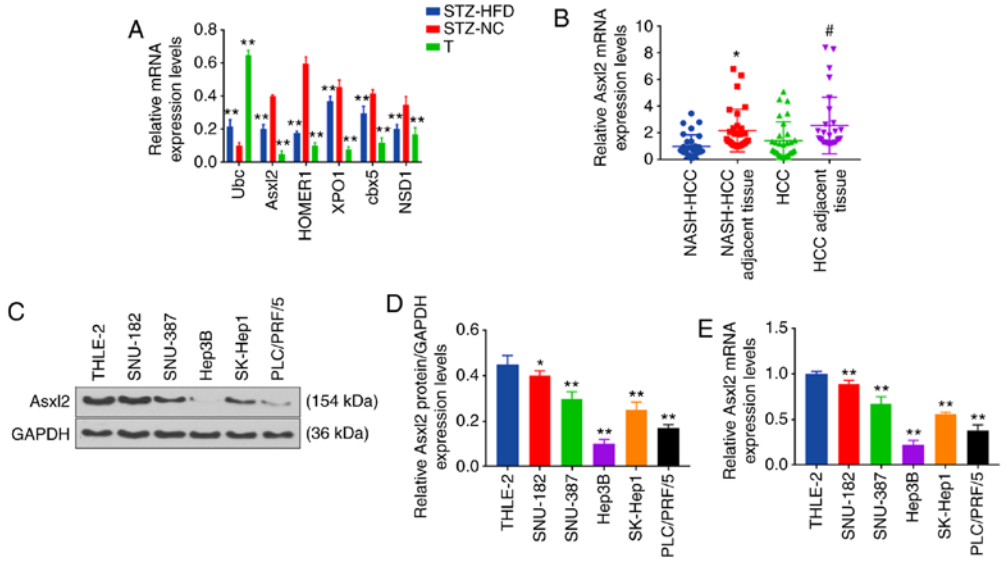

Figure 4. Representative DEGs in NASH-HCC, other HCC and non-cancerous matched tissues from mice or humans. (A) Expression levels of Ubc, Asxl2, HOMER1, XPO1, cbx5, NSD1 in NASH-HCC (tumor, T), normal (STZ-NC group) and non-cancerous matched tissues (STZ-HFD group, n=3 in each group) measured by RT-qPCR. **P<0.001 vs. STZ-NC group. (B) Expression of Asxl2 in human NASH-HCC, NASH-HCC adjacent tissues, HCC and HCC adjacent tissues (n=3/each group) measured by RT-qPCR. *P<0.05 vs. NASH-HCC. $^{\#}$P<0.05 vs. HCC. (C-E) Expression of Asxl2 in human liver epithelial cell line (THLE-2), human liver cancer cell lines (SNU-182, SNU-387, Hep3B, SK-Hep1and PLC/PRF/5) measured by (C and D) western blot analysis and (E) RT-qPCR. *P<0.05, **P<0.001 vs. THLE-2 cells. NASH, non-alcoholic steatohepatitis; HCC, hepatocellular carcinoma; STZ, streptozotocin; HFD, high-fat diet; NC, negative control.

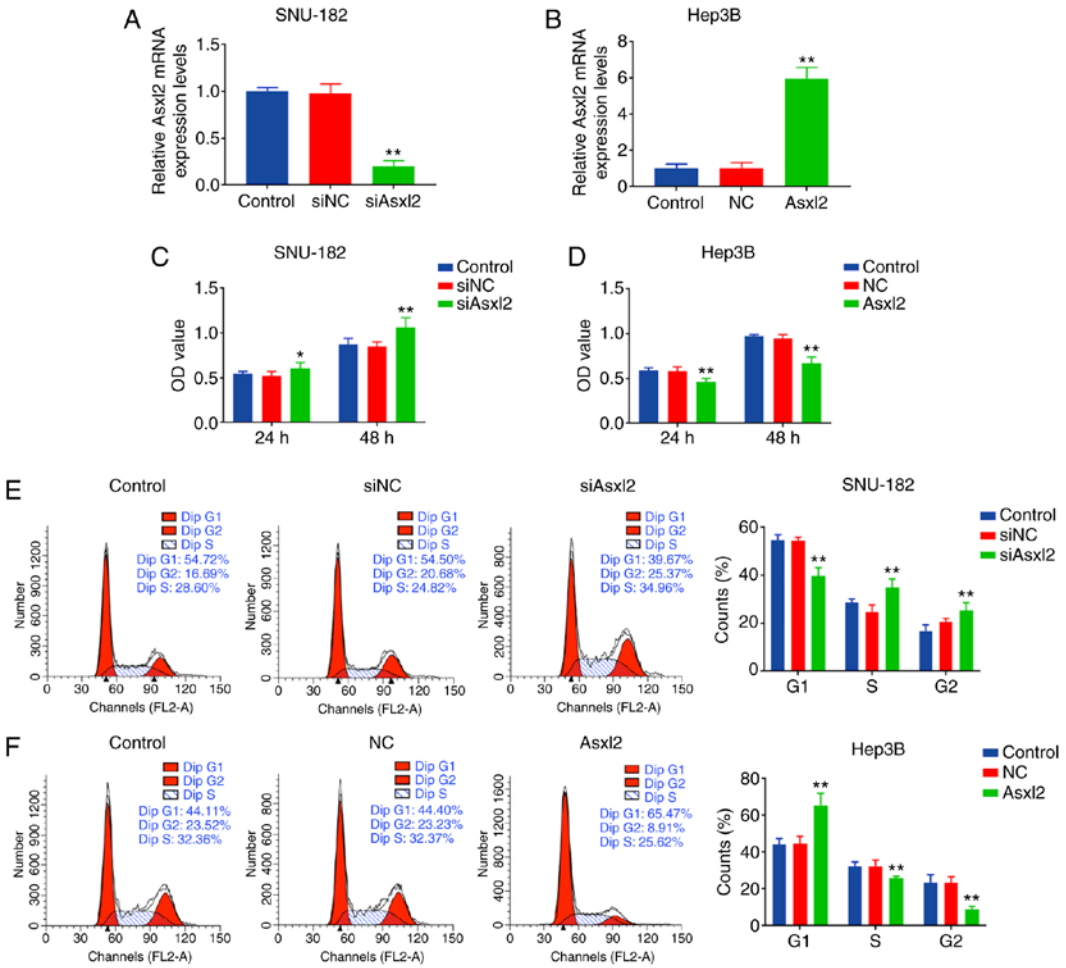

Figure 5. Effects of Asxl2 on the proliferation and cell cycle of SNU-182 and Hep3B cells. (A and B) Expression of Asxl2 in (A) SNU-182 and (B) Hep3B cells following interference with (A) siRNAs or (B) overexpression plasmids measured by RT-qPCR. (C and D) The proliferative ability of the (C) SNU-182 and (D) Hep3B cells following interference with (C) siRNAs or (D) overexpression plasmids was measured by CCK-8 assays. (E and F) The cell cycle of (E) SNU-182 and (F) Hep3B cells following interference with (E) siRNAs or (F) overexpression plasmids measured by flow cytometry. *P<0.05, **P<0.001 vs. siNC or NC. siNC, scramble negative control; NC, empty plasmid.

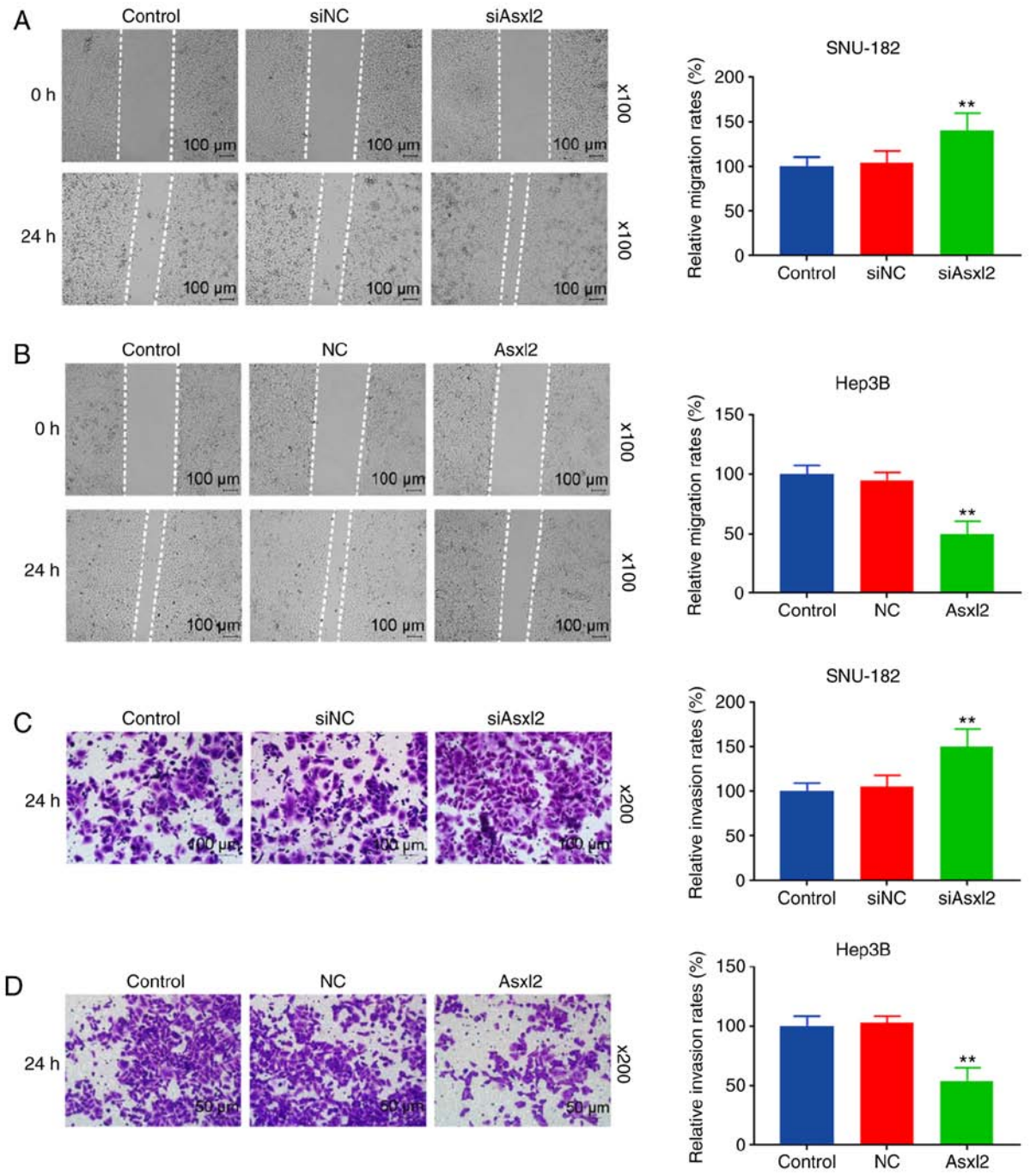

Figure 6. Effects of Asxl2 on the migration and invasion of SNU-182 and Hep3B cells. (A and B) The proliferation of (A) SNU-182 and (B) Hep3B cells following interference with (A) siRNAs or (B) overexpression plasmids measured by CCK-8 assays. (C and D) The cell cycle of (C) SNU-182 and (D) Hep3B cells following interference with (C) siRNAs or (D) overexpression plasmids was measured by flow cytometry. **P<0.001 vs. siNC or NC. siNC, scramble negative control. NC, empty plasmid.

identified. These DEGs were found mainly related to the molecular functions of chromosome organization, mitotic nuclear division and chromatin modification, and pathways of the cell cycle and MAPK. Of note, among these DEGs, Asxl2, which is closely related to glucose and lipid metabolism, was significantly downregulated in NASH-HCC, and regulated the growth, migration and invasion of human HCC cells.

In the present study, NASH-HCC was first induced in ApoE$^{-/-}$ mice by injecting STZ and feeding the mice a HFD, as previously described (26). It was found that the concentration of blood glucose was significantly increased in the STZ-HFD mice, which was consistent with the results of a previous study showing that STZ increased blood glucose (27). The serum levels of the hepatic enzymes, ALT and AST, were measured to indicate liver cell damage (28), and the serum level of TBA was detected as an index of character cholestasis (29). Lipid profiles of TG, TC and LDL accumulations are involved in the pathogenesis of hepatotoxicity (30). Therefore, the present study measured these hepatotoxicity-related parameters, and it was found that mice in the STZ-HFD group showed significant liver injury similar to the findings of a previous study, in which

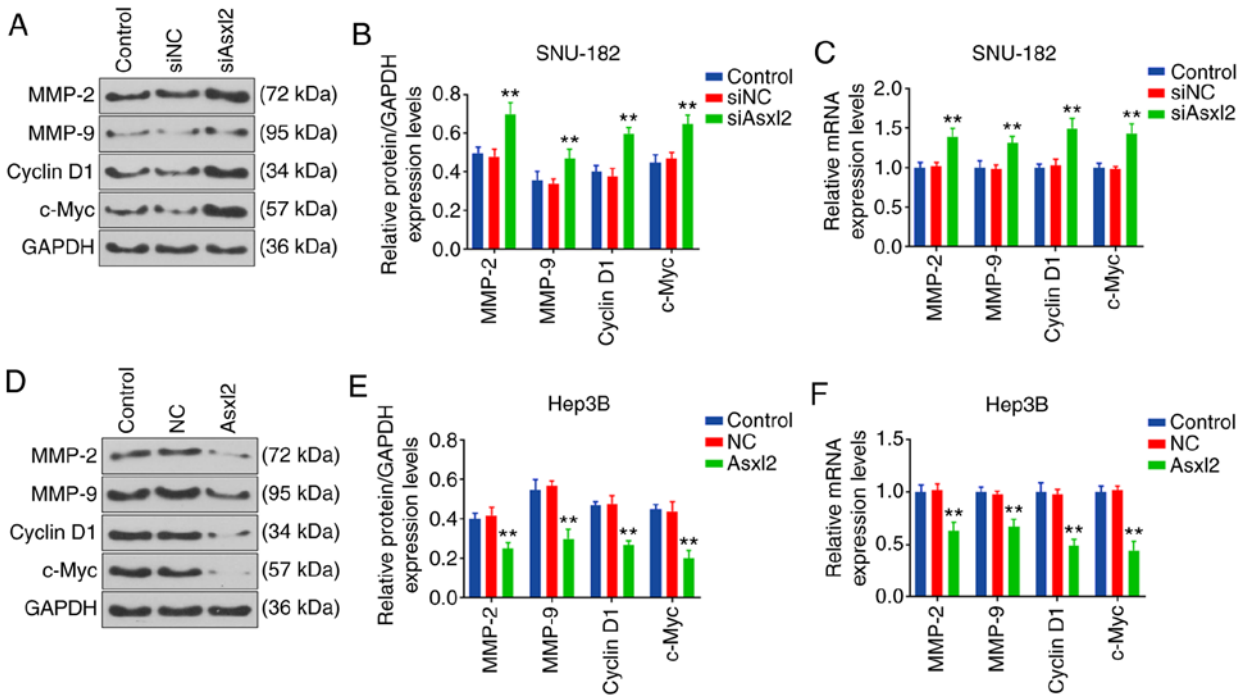

Figure 7. Effects of Asxl2 on cell metastasis and cycle-associated protein expression in SNU-182 and Hep3B cells. (A-C) Expression of MMP-2, MMP-9, cyclin D1 and c-Myc in SNU-182 cells following interference with siRNAs measured by (A and B) western blot analysis and (C) RT-qPCR. (D-F) Expression of MMP-2, MMP-9, cyclin D1 and c-Myc in Hep3B cells following transfection with Asxl2 overexpression plasmid measured by (D and E) western blot analysis and (F) RT-qPCR. **P<0.001 vs. siNC or NC. siNC, scramble negative control; NC, empty plasmid.

the levels of AST, ALT and ALP were found increased in rats with STZ-induced diabetes (31).

The expression levels of pro-inflammatory factors (32,33) were also detected in liver tissues and tumor tissues from mice in the STZ-HFD group, and it was found that the expression levels of IL-6, TNF-α, GPC3 and TGF-β were upregulated in the tumor tissues. Notably, GPC3, a heparan sulfate proteoglycan binding to the cell membrane by glycosylphosphatidylinositol, is hardly expressed in adults, except in the placenta. However, GPC3 expression is specifically upregulated in a number of tumors, including in HCC and is used in immunotherapy (34,35). Notably, it was also found that the collagen type 3 level was upregulated in the liver tissues of mice in the STZ-HFD group, but was decreased in the tumor tissues. Thus, it was considered that the pro-inflammatory response in liver tissues and tumor tissues differed from that of the mice in the STZ-HFD group.

The present study also performed transcriptomic analysis to systematically analyze the differences between normal liver tissues and NASH-HCC tissues. The data revealed significant differences between transcriptomic patterns of normal liver and NASH-HCC. The DGEs were mainly related to chromosome organization, mitotic nuclear division, chromatin modification, DNA repair, mRNA processing and chromosome segregation. In addition, these genes mainly participated in cell cycle, MAPK signaling pathways, platinum drug resistance and the Fanconi anemia pathway. Notably, the cell cycle, MAPK signaling pathways and platinum drug resistance are all closely related to tumor development (36).

The 5 most upregulated genes and the 11 most downregulated genes were identified in NASH-HCC in comparison with normal tissues. Genes, such as Ubc (37), XPO1 (38) and CBX5 have been studied in other tumors (39). HOMER1, which is downregulated in HBV-induced HCC (40), was also identified in the present study. Among these DEGs, Asxl2 expression was the most downregulated in the tumor tissues and it was similarly downregulated in human HCC cell lines. Asxl2 encodes a member of a family of epigenetic regulators involved in the assembly of transcription factors at specific genomic loci. A previous study indicated that Asxl2 was necessary for maintaining steady-state hematopoiesis (41). ASXL2 interacts with peroxisome proliferator-activated receptor (PPAR)γ and PPAR-activated receptor during adipogenesis (42). Of note, a previous study demonstrated that mice with Asxl2 knockout easily develop insulin resistance and lipodystrophy, and fail to respond to a HFD (25), suggesting that Asxl2 may play a role in lipid metabolic comorbidities and diabetes. In the present study, functional experiments revealed that Asxl2 regulated the proliferation, cell cycle, migration and invasion of HCC cells. The levels of MMPs (MMP-2 and MMP-9) are closely related to cell metastasis (43), and cyclin D1 and c-Myc levels are related to the cell cycle (44); thus, these the expression levels of these proteins were determined by WB analysis. The results revealed that Asxl2 was a tumor suppressor in HCC, which is consistent with the findings of a previous study on HSC (24). The loss of Asxl2 is associated with increased chromatin accessibility at putative enhancers of key leukemogenic loci during leukemogenesis (45). The deletion of Asxl2 also affects self-renewal, differentiation and apoptosis of HSC (24). In contrast to the majority of studies, Asxl2 has bene shown to promote the growth of breast cancer cells by regulating ERα target gene expression (46). Therefore, it was considered that Asxl2 acts as an epigenetic regulator

and may regulate important gene networks in various types of cancer.

It should be noted that there were also some limitations to the present study. For example, the signaling pathway involved in the suppressive effects of Asxl2 on the development of NASH-HCC from diabetes was not identified, and this needs to be addressed in future research.

In conclusion, the present study provided a genome-wide gene expression profile of NASH-HCC. Among all the DEGs, Asxl2, which was identified to be a tumor suppressor in HCC, and may play an important role in the development of NASH-HCC developed from diabetes. On the whole, the present study enhances the understanding of the molecular mechanisms responsible for the pathogenesis of NASH-HCC.

Acknowledgements

Not applicable.

Funding

The present study was supported by the Commission of Science Technology of Minhang District (grant no. 2019MHZ079); the Minhang Scientific Research Found Projects Grant (grant no. 2017MHJC02); the Shanghai Science and Technology Fund (grant no. 19142202000).

Availability of data and materials

The analyzed datasets generated during the study are available from the corresponding author on reasonable request.

Authors' contributions

ZH and ZZ made substantial contributions to the conception and design of the study. FT, JF, XW and QC were involved in data acquisition, data analysis and interpretation. ZH and ZZ drafted the article or critically revised it for important intellectual content. All authors gave the final approval of the final version of the manuscript to be published and all authors agree to be accountable for all aspects of the work in ensuring that questions related to the accuracy or integrity of the work are appropriately investigated and resolved.

Ethics approval and consent to participate

All procedures performed in experiments involving human participants were in accordance with the ethical standards of the institutional and/or national research committee and with the 1964 Helsinki declaration and its later amendments or comparable ethical standards. The present study was approved by the Ethics Committee of Minhang Hospital and written informed consent was signed by each participant prior to the surgery. Animal experiments were performed according to the guidelines of Minhang Hospital Animal Ethics Committee. Efforts were made in consideration of animal welfare.

Patient consent for publication

Not applicable.

Competing interests

The authors declare that they have no competing interests.

References

1. Shariff MI, Cox IJ, Gomaa AI, Khan SA, Gedroyc W and Taylor-Robinson SD: Hepatocellular carcinoma: Current trends in worldwide epidemiology, risk factors, diagnosis and therapeutics. Exp Rev Gastroenterol Hepatol 3: 353-367, 2009.
2. Yu Y, Cai J, She Z and Li H: Insights into the epidemiology, pathogenesis, and therapeutics of nonalcoholic fatty liver diseases. Adv Sci (Weinch) 6: 1801585, 2019.
3. Xie G, Wang X, Huang F, Zhao A, Chen W, Yan J, Zhang Y, Lei S, Ge K, Zheng X, *et al*: Dysregulated hepatic bile acids collaboratively promote liver carcinogenesis. Int J Cancer 139: 1764-1775, 2016.
4. Anstee QM, Reeves HL, Kotsiliti E, Govaere O and Heikenwalder M: Gastroenterology HMJNr and hepatology: From NASH to HCC: Current concepts and future challenges. Nat Rev Gastroenterol Hepatol 16: 411-428, 2019.
5. van der Meer AJ, Feld JJ, Hofer H, Almasio PL, Calvaruso V, Fernández-Rodríguez CM, Aleman S, Ganne-Carrié N, D'Ambrosio R, Pol S, *et al*: Risk of cirrhosis-related complications in patients with advanced fibrosis following hepatitis C virus eradication. J Heptol 66: 485-493, 2017.
6. Noureddin M and Rinella ME: Nonalcoholic fatty liver disease, diabetes, obesity, and hepatocellular carcinoma. Clin Cancer Dis 19: 361-379, 2015.
7. Simon TG, King LY, Chong DQ, Nguyen LH, Ma Y, VoPham T, Giovannucci EL, Fuchs CS, Meyerhardt JA, Corey KE, *et al*: Diabetes, metabolic comorbidities, and risk of hepatocellular carcinoma: Results from two prospective cohort studies. Hepatology 67: 1797-1806, 2018.
8. El-Serag HB, Kanwal F, Richardson P and Kramer J: Risk of hepatocellular carcinoma after sustained virological response in Veterans with hepatitis C virus infection. Hepatology 64: 130-137, 2016.
9. El-Shamy A, Eng FJ, Doyle EH, Klepper AL, Sun X, Sangiovanni A, Iavarone M, Colombo M, Schwartz RE, Hoshida Y and Branch AD: A cell culture system for distinguishing hepatitis C viruses with and without liver cancer-related mutations in the viral core gene. J Hepatol 63: 1323-1333, 2015.
10. Setiawan VW, Hernandez BY, Lu SC, Stram DO, Wilkens LR, Marchand LL and Henderson BE: Diabetes and racial/ethnic differences in hepatocellular carcinoma risk: The multiethnic cohort. J Natl Cancer Inst 106: dju326, 2014.
11. Zhang Q, Deng YL, Liu C, Huang LH, Shang L, Chen XG, Wang LT, Du JZ, Wang Y, Wang PX, *et al*: Diabetes mellitus may affect the long-term survival of hepatitis B virus-related hepatocellular carcinoma patients after liver transplantation. World J Gastroenterol 22: 9571-9585, 2016.
12. Chiang CH, Lee LT, Hung SH, Lin WY, Hung HF, Yang WS, Sung PK and Huang KC: Opposite association between diabetes, dyslipidemia, and hepatocellular carcinoma mortality in the middle-aged and elderly. Hepatology 59: 2207-2215, 2014.
13. Shima T, Uto H, Ueki K, Kohgo Y, Yasui K, Nakamura N, Nakatou T, Takamura T, Kawata S and Notsumata K: Hepatocellular carcinoma as a leading cause of cancer-related deaths in Japanese type 2 diabetes mellitus patients. J Gastroenterol 54: 64-77, 2019.
14. de Oliveira S, Houseright RA, Graves AL, Golenberg N, Korte BG, Miskolci V and Huttenlocher A: Metformin modulates innate immune-mediated inflammation and early progression of NAFLD-associated hepatocellular carcinoma in zebrafish. J Hepatol 70: 710-721, 2019.
15. Ye J, Li TS, Xu G, Zhao YM, Zhang NP, Fan J and Wu J: JCAD promotes progression of nonalcoholic steatohepatitis to liver cancer by inhibiting LATS2 kinase activity. Cancer Res 77: 5287-5300, 2017.
16. Vandekerckhove L, Vermeulen Z, Liu ZZ, Boimvaser S, Patzak A, Segers VF and De Keulenaer GW: Neuregulin-1 attenuates development of nephropathy in a type 1 diabetes mouse model with high cardiovascular risk. Am J Physiol Endocrinol Metab 310: E495-E504, 2016.

17. Li M, Dou L, Jiao J, Lu Y, Guo HB, Man Y, Wang S and Li J: NADPH oxidase 2-derived reactive oxygen species are involved in dysfunction and apoptosis of pancreatic β-cells induced by low density lipoprotein. Cell Physiol Biochem 30: 439-449, 2012.
18. Al-Malki AL, Sayed AA and Rabey HA: Proanthocyanidin attenuation of oxidative stress and NF-κB protects apolipoprotein E-deficient mice against diabetic nephropathy. Evid Based Complement Alternat Med 2013: 769409, 2013.
19. Livak KJ and Schmittgen TD: Analysis of relative gene expression data using real-time quantitative PCR and the 2(-Delta Delta C(T)) method. Methods 25: 402-408, 2001.
20. Liao Y, Smyth GK and Shi W: FeatureCounts: An efficient general purpose program for assigning sequence reads to genomic features. Bioinformatics 30: 923-930, 2014.
21. Robinson MD, McCarthy DJ and Smyth GK: EdgeR: A Bioconductor package for differential expression analysis of digital gene expression data. Bioinformatics 26: 139-140, 2010.
22. Hughes FM, Kennis JG, Youssef MN, Lowe DW, Shaner BE and Purves JT: The NACHT, LRR and PYD domains-containing protein 3 (NLRP3) inflammasome mediates inflammation and voiding dysfunction in a lipopolysaccharide-induced rat model of cystitis. J Clin Cell Immunol 7: 396, 2016.
23. Wu J, Mao X, Cai T, Luo J and Wei L: KOBAS server: A web-based platform for automated annotation and pathway identification. Nucleic Acids Res 34: W720-W724, 2006.
24. Li J, He F, Zhang P, Chen S, Shi H, Sun Y, Guo Y, Yang H, Man N, Greenblatt S, *et al*: Loss of asxl2 leads to myeloid malignancies in mice. Nat Commun 8: 15456, 2017.
25. Izawa T, Rohatgi N, Fukunaga T, Wang QT, Silva MJ, Gardner MJ, McDaniel ML, Abumrad NA, Semenkovich CF, Teitelbaum SL and Zou W: ASXL2 regulates glucose, lipid, and skeletal homeostasis. Cell Rep 11: 1625-1637, 2015.
26. Hanssen NM, Brouwers O, Gijbels MJ, Wouters K, Wijnands E, Cleutjens JP, De Mey JG, Miyata T, Biessen EA, Stehouwer CD and Schalkwijk CG: Glyoxalase 1 overexpression does not affect atherosclerotic lesion size and severity in $ApoE^{-/-}$ mice with or without diabetes. Cardiovasc Res 104: 160-170, 2014.
27. Huang MC, Chen LY, Chang HM, Liang XY, Chen CK, Cheng WJ and Xu K: Decreased blood levels of oxytocin in ketamine-dependent patients during early abstinence. Front Psychiatry 9: 633, 2018.
28. Huang Z, Jing X, Sheng Y, Zhang J, Hao Z, Wang Z and Ji L: (-)-Epicatechin attenuates hepatic sinusoidal obstruction syndrome by inhibiting liver oxidative and inflammatory injury. Redox Biol 22: 101117, 2019.
29. El-Hawary SS, Ali ZY and Younis IY: Hepatoprotective potential of standardized ficus species in intrahepatic cholestasis rat model: Involvement of nuclear factor-κB, and farnesoid X receptor signaling pathways. J Ethnopharmacol 231: 262-274, 2019.
30. Parvez MK, Al-Dosari MS, Arbab AH and Niyazi S: The in vitro and in vivo anti-hepatotoxic, anti-hepatitis B virus and hepatic CYP450 modulating potential of cyperus rotundus. Saudi Pharm J 27: 558-564, 2019.
31. Gad-Elkareem MA, Abdelgadir EH, Badawy OM and Kadri A: Potential antidiabetic effect of ethanolic and aqueous-ethanolic extracts of leaves on streptozotocin-induced diabetes in rats. PeerJ 7: e6441, 2019.
32. Kazemi A, Soltani S, Ghorabi S, Keshtkar A, Daneshzad E, Nasri F and Mazloomi SM: Effect of probiotic and synbiotic supplementation on inflammatory markers in health and disease status: A systematic review and meta-analysis of clinical trials. Clin Nutr 39: 789-819, 2019.
33. Azushima K, Uneda K, Wakui H, Ohki K, Haruhara K, Kobayashi R, Haku S, Kinguchi S, Yamaji T, Minegishi S, *et al*: Effects of rikkunshito on renal fibrosis and inflammation in angiotensin II-infused mice. Sci Rep 9: 6201, 2019.
34. Shimizu Y, Suzuki T, Yoshikawa T, Endo I and Nakatsura T: Next-Generation cancer immunotherapy targeting glypican-3. Front Oncol 9: 248, 2019.
35. Ortiz MV, Roberts SS, Bender JG, Shukla N and Wexler LH: Immunotherapeutic targeting of GPC3 in pediatric solid embryonal tumors. Front Oncol 9: 108, 2019.
36. Cohen JV and Sullivan RJ: Developments in the space of new MAPK pathway inhibitors for BRAF-mutant melanoma. Clin Cancer Res 25: 5735-5742, 2019.
37. Liu Y, Yang Z, Du F, Yang Q, Hou J, Yan X, Geng Y, Zhao Y and Wang H: Molecular mechanisms of pathogenesis in hepatocellular carcinoma revealed by RNA-sequencing. Mol Med Rep 16: 6674-6682, 2017.
38. Birnbaum DJ, Finetti P, Birnbaum D, Mamessier E and Bertucci F: Expression is a poor-prognosis marker in pancreatic adenocarcinoma. J Clin Med 8: 596, 2019.
39. Vad-Nielsen J, Jakobsen KR, Daugaard TF, Thomsen R, Brügmann A, Sørensen BS and Nielsen AL: Regulatory dissection of the CBX5 and hnRNPA1 bi-directional promoter in human breast cancer cells reveals novel transcript variants differentially associated with HP1α down-regulation in metastatic cells. BMC Cancer 16: 32, 2016.
40. Luo P, Feng X, Jing W, Zhu M, Li N, Zhou H, Worley PF, Chai H and Tu J: Clinical and diagnostic significance of Homer1 in hepatitis B virus-induced hepatocellular carcinoma. J Cancer 9: 683-689, 2018.
41. Madan V, Han L, Hattori N, Teoh WW, Mayakonda A, Sun QY, Ding LW, Nordin HB, Lim SL and Shyamsunder P: ASXL2 regulates hematopoiesis in mice and its deficiency promotes myeloid expansion. Haematologica 103: 1980-1990, 2018.
42. Park UH, Yoon SK, Park T, Kim EJ and Um SJ: Additional sex comb-like (ASXL) proteins 1 and 2 play opposite roles in adipogenesis via reciprocal regulation of peroxisome proliferator-activated receptor {gamma}. J Biol Chem 286: 1354-1363, 2011.
43. Hung CY, Lee CH, Chiou HL, Lin CL, Chen PN, Lin MT, Hsieh YH and Chou MC: Praeruptorin-B inhibits 12-O-tetradecanoylphorbol-13-acetate-induced cell invasion by targeting AKT/NF-κB via matrix metalloproteinase-2/-9 expression in human cervical cancer cells. Cell Physiol Biochem 52: 1255-1266, 2019.
44. Chen L, Zhu D, Feng J, Zhou Y, Wang Q, Feng H, Zhang J and Jiang J: Overexpression of HHLA2 in human clear cell renal cell carcinoma is significantly associated with poor survival of the patients. Cancer Cell Int 19: 101, 2019.
45. Micol JB, Pastore A, Inoue D, Duployez N, Kim E, Lee SC, Durham BH, Chung YR, Cho H, Zhang XJ, *et al*: ASXL2 is essential for haematopoiesis and acts as a haploinsufficient tumour suppressor in leukemia. Nat Commun 8: 15429, 2017.
46. Park UH, Kang MR, Kim EJ, Kwon YS, Hur W, Yoon SK, Song BJ, Park JH, Hwang JT, Jeong JC and Um SJ: ASXL2 promotes proliferation of breast cancer cells by linking ERα to histone methylation. Oncogene 35: 3742-3752, 2016.